Multitracer determination of apparent groundwater ages in peridotite aquifers within the Samail ophiolite, Sultanate of Oman

Amelia N. Paukert Vankeuren[a,b], Jürg M. Matter[a,c], Martin Stute[a,d], Peter B. Kelemen[a,e]

[a]Lamont-Doherty Earth Observatory, Columbia University, 61 Route 9W, Palisades, NY 10964

[b]Geology Department, California State University, Sacramento, 6000 J Street, M/S 6043, Sacramento CA 95819

[c]Ocean and Earth Science, National Oceanography Centre Southampton, University of Southampton, UK

[d]Department of Environmental Science, Barnard College, 3009 Broadway, 404 Altschul Hall, New York, NY 10027

[e]Department of Earth and Environmental Sciences, Columbia University, New York, NY 10027

Corresponding author:
Amelia N. Paukert Vankeuren
California State University, Sacramento
6000 J Street, M/S 6043
Sacramento, CA 95819-6043
Vankeuren@csus.edu
1-916-278-7385

Keywords
CO_2 sequestration
Peridotite
Environmental tracer
Noble gas
Hydrogeology
Water-rock interaction

Abstract

CO_2 sequestration in the form of carbonate minerals via alteration of oceanic crust and upper mantle is an important part of the global carbon cycle, but the annual rate of CO_2 mineralization is not well quantified. This study aimed to constrain groundwater ages within the Samail ophiolite, Sultanate of Oman. Such ages could provide upper bounds on the time required for ongoing low temperature CO_2 mineralization. While we were able to estimate apparent

groundwater ages for modern waters, results from hyperalkaline boreholes and springs were disappointing. Waters from boreholes and hyperalkaline springs within the ophiolite were characterized using multiple environmental tracers including tritium (^{3}H), noble gases (^{3}He, ^{4}He, Ne, Ar, Kr, Xe), stable isotopes ($\delta^{18}O$, $\delta^{2}H$), and chemical parameters (pH, Ca, Mg, DIC, etc.). Shallow peridotite groundwater and samples from boreholes near the mantle transition zone have a pH < 9.3, are 4-40 years old, have little to no non-atmospheric He accumulation, NGTs (noble gas temperatures) equivalent to the modern mean annual ground temperature, and stable isotopes within the range of current local precipitation. In contrast, hyperalkaline springs and deeper samples from peridotite boreholes have pH > 10, are pre-H-bomb (older than 1952), have significant non-atmospheric helium accumulation (30 -70% of dissolved helium), often are isotopically heavier (enriched in $\delta^{18}O$), and can have NGTs 6-7^{o}C lower than the modern ground temperature. These differences suggest that groundwater in deep (> 50 m) peridotite aquifers is considerably older than shallow groundwater in peridotite and water in deeper aquifers near the mantle transition zone. Unfortunately, how much older remains an open question. The low NGT of groundwater from one deep (300 m) peridotite borehole indicates it is probably glacial in origin. If so, it must date back to at least the late Pleistocene, the most recent glacial period; He accumulation suggests it could be from 20-220 ka. The inefficacy of this suite of environmental tracers to quantitatively estimate apparent groundwater age for hyperalkaline fluids necessitates the use of different techniques. Future work to constrain groundwater ages should utilize a packer system to isolate discrete depth intervals within boreholes and less common environmental tracers such as ^{39}Ar and ^{81}Kr.

1. Introduction

1.1 Natural carbon storage via seafloor alteration

Quantifying the natural global carbon budget is a key piece of the climate change puzzle, as we must understand the natural system in order to quantify the impact of human influence. One aspect of the global carbon budget is sequestration in the form of carbonate minerals due to alteration of oceanic crust and upper mantle by reacting with circulating ocean water. During this process, alteration of peridotite to form serpentine and carbonate minerals results in an average concentration on the order of 0.1 to 0.2 wt % C (e.g., Kelemen and Manning, 2015; Kelemen et al., 2011 and references therein), though the process can generate ophicalcites with up to 9.6 wt % C (e.g., Agrinier et al., 1988; Schwarzenbach et al., 2013). Because of the large volumes of peridotite exposed to seawater alteration, the process is estimated to sequester 1.5-150 x 10^6 metric tons CO_2/yr (tCO_2/yr) (e.g., Alt and Teagle, 1999; Kelemen et al., 2011; Alt et al., 2013; Schwarzenbach et al., 2013; Kelemen and Manning 2015).

The rate of CO_2 mineralization – conversion of CO_2 to carbonate minerals for permanent storage – is controlled by the rate of water-peridotite reaction and depends on a variety of factors including availability of dissolved CO_2, reactive surface area of peridotite, and kinetics of geochemical reactions. Fluid transport affects all three of these factors, and thus it is critical to characterize the flow regime beneath the surface. Studies have provided valuable insight into flow and transport properties of the upper portion of oceanic crust (e.g., Wheat et al., 2000; Fisher et al., 2003; Hutnak et al., 2006; Winslow et al., 2016; Neira et al., 2016). However, it is unlikely that fluid flow through volcanic basalt is representative of that through fractured peridotite. It is not yet technologically feasible to conduct field studies of reaction rates within peridotite of the upper mantle, but ophiolites – portions of oceanic crust and upper mantle thrust onto a continent during tectonic collisions – offer more accessible field laboratories in which to measure CO_2 mineralization.

Aquifers in the peridotite section of the Samail ophiolite in the Sultanate of Oman are sites of ongoing low-temperature alteration: circulation of meteoric water containing atmospheric CO_2 causes both serpentinization and CO_2 mineralization. Natural CO_2 mineralization within the Samail ophiolite is thought to sequester up to 10^5 tCO_2/yr of atmospheric carbon dioxide in the form of carbonate minerals (Kelemen and Matter, 2008). This estimate for CO_2 mineralization rate is based on the abundance and age of carbonate terraces and veins; it doesn't include constraints from the flow rate of groundwater and the reactive surface area of the peridotite.

Groundwater age and chemistry could provide additional constraints on the rate of natural CO_2 mineralization. When water enters the groundwater system, it carries dissolved carbon from interaction with the atmosphere and soil CO_2. Along its flow path, as the water reacts with peridotite to form serpentine, the reaction releases Mg^{2+} and Ca^{2+} into the water (Eq. 1), which then combines with the dissolved carbon to form magnesite, dolomite and calcite (e.g., Eq. 2). This process continues until dissolved carbon is depleted, at which point Ca^{2+} begins to accumulate and greater extents of water-rock reaction produce high concentrations of dissolved Ca^{2+} and high pH, often reaching hyperalkaline values (pH 11-12).

$$4Mg_2SiO_4 + CaMgSi_2O_6 + 7H_2O \rightarrow 3Mg_3Si_2O_5(OH)_4 + Ca^{2+} + 2OH^- \quad (1)$$

$$Ca^{2+} + HCO_3^- \rightarrow CaCO_3 + H^+ \quad (2)$$

The chemistry of hyperalkaline spring waters in the Samail ophiolite (pH > 11, high Ca^{2+}, depleted in dissolved inorganic carbon) suggests that all dissolved CO_2 in the water has been mineralized (e.g., Neal and Stanger, 1985; Paukert et al., 2012). Groundwater flow controls CO_2 transport, so groundwater age provides the maximum amount of time during which mineralization of dissolved CO_2 could have taken place. This leaves reactive surface area and reaction kinetics as unknown variables controlling reaction rates. If we assume that reaction

kinetics in the aquifers are comparable to those measured in laboratory settings, geochemical modeling can be used to calculate the minimum amount of reactive surface area necessary to produce the reaction rate per kg of peridotite that achieves complete mineralization of dissolved CO_2 in the timeframe of the apparent groundwater age.

Most CO_2 mineralization appears to occur in the upper 50 m of the peridotite, where the groundwater is closer to the atmosphere and may absorb atmospheric and soil CO_2 (Kelemen and Matter, 2008). However, additional mineralization occurs in veins at depth and in carbonate terraces when hyperalkaline water emerges at the surface and absorbs CO_2 from the atmosphere. Reaction path modeling of water-rock interaction in Oman peridotite conducted by Paukert et al. (2012) suggests that natural CO_2 mineralization at depth in aquifers closed to atmospheric exchange is limited by the amount of dissolved CO_2 in infiltrating groundwater. Thus, flow rate controls CO_2 mineralization at depth, as well as at the surface through the amount of hyperalkaline fluid emitted by springs and therefore available to react with atmospheric CO_2. The modeling also showed CO_2 mineralization may occur relatively quickly - with dissolved CO_2 being removed from the groundwater after 600 years of water-rock reaction - after which the groundwater continues to interact with and serpentinize the peridotite for another ~6,000 years before it attains a pH of 12. The ubiquity of hyperalkaline springs emerging from the Oman peridotite (Neal and Stanger, 1983; 1985) is thus inferred to result from generally long residence times for waters within the peridotite aquifer. This presents a complication: if CO_2 mineralization is concentrated in the early years of groundwater circulation, the minimum reaction rate for CO_2 mineralization (and associated reactive surface area) calculated from the apparent groundwater age would be a significant underestimate.

Because serpentinization continues to occur after dissolved CO_2 has all been mineralized, serpentinization rate estimates may provide better constraints on reactive surface area. Serpentinization in the absence of dissolved CO_2 causes a rise in pH and accumulation of Ca^{2+} in the fluid (Eq. 1). Again, using the apparent groundwater age as a maximum duration of water-rock reaction, together with laboratory-determined kinetic rates, geochemical modeling can be used to calculate the minimum serpentinization rate and reactive surface area necessary to generate the observed pH and concentration of dissolved Ca^{2+} in the groundwater. The reactive surface area calculated from serpentinization can then be used as an input for geochemical models to better estimate the CO_2 mineralization rate.

Either method for estimating alteration rate and peridotite reactive surface area requires accurate determination of groundwater age to constrain the maximum reaction time. Thus, a better understanding of groundwater ages in the Samail ophiolite aquifer could offer valuable information on natural CO_2 mineralization rates and reactive surface area in peridotite that could be applicable both to other ophiolites and at the seafloor.

1.2 Natural and engineered carbon storage via CO_2 mineralization in ophiolites

In addition to providing insight into the natural CO_2 mineralization process, the Samail ophiolite has been proposed as a site for an engineered geological CO_2 storage project (e.g., Kelemen and Matter, 2008; Kelemen et al., 2011). With approximately 50×10^{12} metric tons of peridotite (Kelemen and Matter, 2008), the Samail Ophiolite has the capacity to mineralize about 30×10^{12} tCO_2 if fully carbonated. At the 2015 global rate of emissions of 36.3×10^9 tCO_2/year (Le Quéré et al., 2016), that would theoretically be enough to sequester over 800 years' worth of anthropogenic CO_2 emissions. Though it is unlikely that the Samail ophiolite will be fully

153 carbonated, there is still the potential for significant CO_2 storage if the rate of CO_2 mineralization
154 can be increased.
155 Engineered *in situ* CO_2 mineralization in mafic geologic formations shows promise. Pilot
156 projects in Wallulla, WA and near Reykjavik, Iceland have demonstrated rapid (< 2 years) CO_2
157 mineralization in basaltic rocks (e.g., Matter et al., 2016; McGrail et al., 2017; Snæbjörnsdóttir et
158 al., 2017). With equivalent reactive surface area, peridotite could produce even faster reactions
159 and CO_2 mineralization than basaltic rocks (Kelemen et al., 2011). However, as with natural
160 CO_2 mineralization, the reaction rate will be constrained by the amount of reactive surface area
161 among other factors (e.g. temperature, CO_2 supply rate). Reactive transport modeling of
162 dissolved CO_2 injection into the peridotite section of the Samail Ophiolite suggests that
163 maximizing CO_2 mineralization rates would require careful tuning of the CO_2 injection rate to
164 the reactive surface area (Paukert, 2014). Thus, in order to accurately predict the CO_2 storage
165 potential and design a pilot project, it is necessary to first quantify the amount of reactive surface
166 area.
167 *1.3 Geologic setting*
168 The Samail ophiolite is the largest in the world, with approximately 15,000 km^3 of peridotite
169 within a few kilometers of the surface (Nicolas et al., 2000; Kelemen and Matter, 2008). The
170 Samail ophiolite aquifer is hosted by fractured crystalline rock with most of the porosity and
171 permeability in fractures (Dewandel et al., 2005) and much of the matrix potentially shielded
172 from interaction with aquifer fluid. Peridotite from the Samail ophiolite contains veins and
173 fractures on a wide variety of scales, from larger fractures and veins with meter spacing down to
174 serpentine-filled veins with 10 micron spacing (Kelemen et al., 2011). Water flow within
175 peridotite aquifers of the Samail ophiolite is dominated by larger fractures and fissures

(Dewandel et al., 2005). However, the reactive surface area is likely dominated by the smaller, 10 to 100 micron scale fractures and veins (hereafter referred to as microcracks). Microcracks also constitute pathways for fluid circulation, allowing less flow than larger fractures, but more flow than the peridotite matrix.

1.4 Apparent groundwater ages

Previous attempts to constrain the age of water in aquifers in the peridotite section of the Samail ophiolite have been unsuccessful. $^{3}H/^{3}He$ dating of hyperalkaline springs provides a minimum age, as spring waters have <0.6 TU and therefore must have recharged prior to 1952. Radiocarbon dating of spring water has been unsuccessful, as the hyperalkaline water is so depleted in dissolved carbon (e.g., Neal and Stanger, 1983; Neal and Stanger 1985; Paukert et al. 2012) that it is difficult to get enough material to date. Also, when exposed to air these carbon-poor hyperalkaline waters rapidly absorb atmospheric carbon dioxide with modern ^{14}C values so samples are easily contaminated by the modern signal (see ^{14}C data in the Supporting Information). Additionally, if the spring waters experience mixing with shallow groundwater during their migration to the surface, their ^{3}H and carbon content may be dominated by the modern component.

Due to the limited success of some groundwater dating techniques, this study used a variety of environmental tracers: ^{3}H, noble gases (He, Ne, Ar, Kr, Xe), and stable isotopes ($\delta^{18}O$, $\delta^{2}H$) as well as water chemistry to constrain apparent groundwater age (detailed discussion of hyperalkaline spring and shallow groundwater chemistry can be found in Paukert et al., 2012). Additionally, water samples were collected from boreholes in the peridotite to avoid the effects of mixing between deep groundwater and waters in the shallow subsurface, as may occur along

198 the flow path of spring water. These data are used to estimate the ages of waters in different
199 settings in the ophiolite, which may then be used to constrain natural CO_2 mineralization rates.

200 **2. Methods**

201 *2.1 Environmental tracers*

202 *2.1.1 $^3H/^3He$ dating*

203 ^3H is commonly used for identifying modern groundwater: water recharged after the advent
204 of atmospheric thermonuclear testing in 1952. ^3H concentration in precipitation peaked at more
205 than 1,000 TU in 1963 (Fig. 1), but subsequent radioactive decay to ^3He and attenuation from
206 mixing with oceans and groundwater caused ^3H in precipitation in the northern hemisphere to
207 approach steady state by the early-mid 1990s (Rozanski, 1991). ^3H ages can be calculated using
208 Eq. 3:

209 $$^3H\ Age = -(t_{1/2}/\ln(2))*\ln(^3H/^3H_{init}) \quad (3)$$

210 where $t_{1/2}$ is the half-life of ^3H (12.3 years), ^3H is the concentration of ^3H measured in the
211 sample, $^3H_{init}$ is the concentration of ^3H at the time of recharge. However, due to decay, current
212 ^3H concentrations in groundwater recharged at any point in the last few decades would show
213 little variation (Fig. 1). Fortunately, $^3H/^3He$ dating allows more accurate determination of
214 apparent groundwater age (Eq. 4; Tolstikhin and Kamensky,1969):

215 $$^3H/^3He\ Age = (t_{1/2}/\ln(2))*\ln(1+^3He_{trit}/^3H) \quad (4)$$

216 where $^3He_{trit}$ is the concentration of ^3He in the sample produced by ^3H decay.

217 *2.1.2 Noble gas thermometer*

218 Dissolved noble gases Ne, Ar, Kr, Xe can be used as a thermometer for the mean annual
219 ground temperature at the time of recharge (e.g., Mazor, 1972; Stute and Schlosser, 1993;
220 Aeschbach-Hertig et al., 1999). Typically, the apparent groundwater age is established through

221 other dating methods (e.g., radiocarbon) and the noble gas temperature (NGT) is used to
222 reconstruct paleotemperatures. However, in the case of the peridotite aquifers in Oman where
223 other dating techniques have been unsuccessful, we may be able to compare NGT to the
224 estimated variation of atmospheric temperature with time (e.g., Clark et al., 1997; Weyhenmeyer
225 et al., 2000; Fleitmann and Matter, 2009; Morrissey et al., 2010) in order to constrain the
226 apparent groundwater age.

227 *2.1.3 Non-atmospheric helium accumulation*

228 He concentration in groundwater typically increases with time and can be used to estimate
229 apparent groundwater age when combined with a He flux (e.g., Torgersen and Ivey, 1985; Stute
230 et al., 1992; Torgersen and Stute, 2013). This technique has been used qualitatively in other areas
231 of Oman (Müller et al., 2016). He can accumulate in groundwater from a variety of sources: *in*
232 *situ* production, crustal flux, mantle flux, tritiogenic production, and release from aquifer
233 formation rocks by enhanced diffusion or mineral dissolution (e.g., Stute et al., 1992; Solomon et
234 al., 1996; Torgersen and Stute, 2013). The $^{3}He/^{4}He$ ratio is different in different sources, and can
235 be used to differentiate between the different He components in some cases (e.g., Torgersen and
236 Stute, 2013 and references therein).

237 *2.1.4 Stable isotopes*

238 Stable isotopes ($\delta^{18}O$, $\delta^{2}H$) in water are commonly used to determine water vapor source.
239 Stable isotopes in meteoric water generally become depleted in heavy isotopes with increasing
240 latitude, distance from the vapor source, and amount of rainout (e.g., Rozanski et al., 1993 and
241 references therein). In Oman, there are two primary vapor sources: a northern, Mediterranean
242 source that dominates during the winter, and a heavier, $\delta^{18}O$ enriched southern, Indian Ocean
243 source that dominates during the summer (Weyhenmeyer et al., 2002). Though the northerly

244 source is currently the predominant one, a weakening of that system during the last glacial
245 maximum is thought to have shifted the primary vapor source to that from the south
246 (Weyhenmeyer et al., 2000). Stable isotopes in Oman groundwater may be used to differentiate
247 between modern water primarily sourced from the north vs. glacial-aged water primarily sourced
248 from the south.

249 *2.2 Field sampling methods*

250 Sampling was conducted over multiple field seasons, from 2009 to 2012. Water samples and
251 dissolved noble gas samples were collected from five deep (200-350 m) boreholes set in the
252 ophiolite (four in peridotite and one in gabbro), three shallow boreholes (< 60 m) in peridotite or
253 peridotite alluvium, and five hyperalkaline spring outlets in peridotite, comprising a total of 12
254 different field sites (two shallow boreholes were co-located) (Table 1, Fig. 2).

255 For deep boreholes, water samples for ^{3}H, water chemistry, and stable isotope analysis were
256 collected without purging the borehole, using a point-source stainless steel bailer with a check-
257 valve both above and below the sample to prevent mixing with shallower water as the sample is
258 raised to the surface. Shallow ground water samples were collected using a submersible pump
259 and spring samples were drawn directly from spring outlets with syringes. Stable isotope and
260 water chemistry samples were filtered to 0.2 μm in the field and samples for major cation and
261 trace element analysis were acidified. Alkalinity was measured in the field using a two-step
262 titration process to distinguish between carbonate alkalinity and hydroxide alkalinity.

263 Noble gas samples from deep boreholes were collected in air-tight copper tubes (Weiss,
264 1968) using a borehole *in situ* sampling device modified from Solomon (1992) with a simple
265 check valve operated by an ultrahigh purity nitrogen cylinder. After lowering the copper tube
266 down the borehole to the sampling depth, pressure in the nitrogen line was reduced to open the

check valve and allow water to enter the sampling line to the height of the water column. The system was then repressurized and brought to the surface to be sealed. Noble gas samples from shallow boreholes and hyperalkaline springs were collected using a submersible typhoon pump and peristaltic pump, respectively.

2.3 Analytical methods

^{3}H and noble gases were measured at Lamont-Doherty Earth Observatory (Ludin et al., 1997; Stute et al., 1995). Analytical precision was better than 2% (standard deviation 1σ) for samples with > 1 TU, 15-30% for samples with < 0.1 TU, 3% for helium, and 1% for neon, argon, krypton, and xenon.

Major ions and dissolved inorganic carbon were measured at Columbia University, Barnard College, and Queens College. Analytical precision was 4% or better (standard deviation 1σ). Trace elements were measured at Arizona State University, and stable isotopes ($\delta^{18}O$ and $\delta^{2}H$) were measured in the Environmental Isotopes Laboratory at the University of Waterloo.

2.4 Statistical methods

Noble gas concentrations were modeled using NOBLE90, a non-linear, error-weighted least squares inversion program that fits measured noble gas concentrations with respect to pressure, salinity, excess air, and fractionation (Aeschbach-Hertig et al., 1999). Heavier noble gases were used to calculate helium due to excess air and non-atmospheric sources. See Supporting Information for more detailed information about model inputs.

3 Results and discussion

3.1 $^{3}H/^{3}He$ dating

Waters with pH < 9.3 have ^{3}H concentrations > 0.6 TU, while waters with pH > 9.3 have < 0.6 TU (Table S1, Fig. 3). Given the ^{3}H concentrations in local precipitation over time, any

water recharged post-1952 would have a ^{3}H concentration of 0.6 TU or higher (Fig. 1). All waters with pH > 9.3 can therefore be classified as pre-bomb recharge mixed with varying fractions of modern water.

The ^{3}H concentration in Oman precipitation has not been directly measured, but can be inferred from the nearest IAEA/WMO Global Network of Isotopes in Precipitation monitoring station, in Bahrain. Bahrain is less than 1000 km to the northwest of Oman and at similar elevation. Precipitation in Bahrain and northern Oman appear to have originated from the same water source and experienced similar transport histories (Weyhenmeyer et al., 2002; Macumber, 2003; Matter et al., 2005). Bahrain modern precipitation varies between 1.6 and 4 TU interannually, with an average value of 3 TU (IAEA, 2018). It is not possible to identify the exact source function for ^{3}H in precipitation in Oman, but for calculations of apparent groundwater age the modern value is taken to be 3 TU.

$^{3}H/^{3}He$ dating (Eq. 4) was applied to samples with > 0.6 TU. To isolate $^{3}He_{trit}$, ^{3}He from solubility equilibrium and excess air were calculated using NOBLE90 and subtracted from total ^{3}He (Aeschbach-Hertig et al., 1999). Very young samples had negative surplus ^{3}He estimates, but these values were within error. For these samples, apparent groundwater ages were calculated using Eq. 3 with a $^{3}H_{init}$ value of 3.

Waters from peridotite boreholes (WDA 05, WDA 17, SJA 4B) had $^{3}H_{init}$ (calculated from $^{3}H+^{3}He_{trit}$) values of 3 to 11 TU and apparent ages ranging from 13 to 37 years, while waters from the gabbro borehole (WDA 16) were younger, with an apparent age of 4 years. When $^{3}H_{init}$ versus $^{3}H/^{3}He$ age is plotted on the Bahrain ^{3}H curve, the samples fall along the local precipitation line indicating that they have not undergone significant mixing and that the $^{3}H/^{3}He$ apparent ages are reliable (Fig. 1).

For waters with pre-bomb ^{3}H concentrations, mixing calculations were performed assuming a modern ^{3}H value of 3 TU and an old ^{3}H value of 0 TU. Hyperalkaline waters contain ^{3}H concentrations at 0.2 – 6% of the modern value, suggesting small amounts of mixing with modern water. One pre-bomb borehole sample, SJA 3B, has a ^{3}H concentration that is 18% of the modern value. The higher degree of mixing with modern water at this site may be due to the shallow depth of the borehole (30 m). Surface water in Oman frequently alternates between flowing in wadis (ephemeral streams) and infiltrating into the shallow subsurface where it could mix with older groundwater.

Within boreholes, there does not appear to be a relationship between $^{3}H/^{3}He$ apparent age and sample depth, either within the same borehole or in aggregate. Within the same borehole, there may not be much variation in apparent age with depth if water in the borehole is dominated by input from a single fracture. When one fracture is significantly more conductive than surrounding ones, most fluid in the borehole will originate from that fracture and reflect the apparent age of that source fluid. A shallow, highly conductive fracture could be responsible for the young apparent age of water at all three depths in borehole WDA 16, which is the deepest borehole and yet has the youngest $^{3}H/^{3}He$ apparent ages (less than 5 years old). Alternatively, the young apparent age of WDA 16 water may be due to the lithology of the borehole: WDA 16 is in gabbro while all other sampled boreholes are in peridotite. In the Samail ophiolite, gabbro is estimated to have hydraulic conductivity 1 to 2 orders of magnitude higher than peridotite (Dewandel et al., 2005), which would potentially allow correspondingly faster flow.

3.2 Water chemistry

Waters generally group into one of two compositions commonly seen in ultramafic settings: Type I Mg^{2+}-HCO_3^- water and Type II Ca^{2+}-OH^- water (e.g., Barnes and O'Neil, 1969; Neal and

Stanger, 1985; Bruni et al., 2002). Our Type I water has pH < 10, relatively low Na^+ and Cl^- (0.7-2 mmol/l) and Ca^{2+} (<0.5 mmol/l), and high Mg^{2+} and DIC (1.5-3 mmol/l) (Table 1 and 2). Our Type II water has pH > 10.5, relatively high Na^+ (10 – 14 mmol/l), Cl^- (14-40 mmol/l) and Ca^{2+} (4-14 mmol/l), but low Mg^{2+} and DIC (<0.5 mmol/l). The shallowest sample from borehole NSHQ 14 is intermediate between these two types.

Almost all Type I waters have modern $^3H/^3He$ apparent ages, while all Type II water samples are pre-bomb (Fig. 3). The relationship between groundwater apparent age and water composition fits water-rock interaction models in which increasing extent of reaction with olivine and pyroxene causes an increase in pH, as in Eq. 1.

All waters with pH less than 8 are young, recharged within the last 20 years. Waters with pH between 9 and 9.3 are modern, recharged between 20 and 40 years ago. This suggests that less than 20 years of water-rock interaction are required in order to generate a pH of 9, consistent with the evolution of pH with time predicted by reaction path modeling of peridotite-water interaction (Paukert et al., 2012). All waters with pH above 9.3 are pre-bomb, suggesting that it requires at least 60 years for water-rock interaction to produce pH 11 water. This number is a minimum estimate: reaction path modeling predicted that it might take 500 – 6,500 years to develop pH 11–12 water (Paukert et al., 2012), though the kinetic data used to constrain that modeling are highly uncertain.

3.3 Dissolved noble gases

Noble gas concentrations for each sample (Table 3) were fitted with models in NOBLE90 (Aeschbach-Hertig et al., 1999). Calculated NGTs and excess air components, as well as selected NOBLE90 models, probabilities, and model uncertainties are given in Table 4. Modeled NGT uncertainties were all below 1°C (Table 4). Uncertainties in salinity, recharge elevation,

and model choice in NOBLE90 added additional uncertainties in recharge temperature of up to 2°C (for all samples except Misbit), but as these factors each push the entire dataset in the same direction, they do not affect relative differences between samples (see Supporting Information for detailed examination of uncertainties). Misbit spring had greater uncertainty in recharge elevation and thus a larger uncertainty in recharge temperature. Three of the five hyperalkaline spring samples and one borehole sample did not have an acceptable fit, so recharge temperatures from these samples are not presented.

3.3.1 Excess air

All borehole water samples contained excess air, as evidenced by neon being present in quantities 1.21-1.93 times solubility equilibrium (R_{Ne}, Table 3). This range is typical of groundwater, which commonly contains up to 85% excess air (Heaton and Vogel, 1981).

Excess air in the Samail Ophiolite aquifer may be particularly high due to the recharge pattern. Northern Oman is an arid environment that sporadically experiences heavy rainfall. Such intermittent recharge events considerably raise the water table and lead to entrapment and (partial) dissolution of air bubbles (Heaton and Vogel, 1981). Large amounts of excess air could also be produced by rapid infiltration of water without a dramatic increase in the water table: in artificial recharge areas the accelerated transport of water to depth is thought to carry entrapped bubbles and cause greater dissolution of excess air (Cey et al., 2008).

The two hyperalkaline spring samples that had acceptable model probabilities contained excess air, though less than the borehole samples, with Ne at 1.02 to 1.20 times solubility. The three hyperalkaline spring samples that could not be successfully modeled had no excess air and neon concentrations 0.27-0.87 times solubility. This provides evidence that these three samples must have undergone extensive degassing. Though a closed-system equilibration model has

been shown to be effective for some degassed water samples (e.g., Aeschbach-Hertig et al., 2008), unfortunately our degassed spring samples could not be fitted by the model.

Hyperalkaline spring waters probably originally contained excess air amounts similar to the borehole samples, but lost dissolved gases as they returned to the surface, prior to reaching the spring outlet. Hyperalkaline springs in areas of peridotite serpentinization are known to have active bubbling of hydrogen and/or methane (e.g., Neal and Stanger, 1983; Chavagnac et al. 2013; Etiope et al., 2013, Miller et al., 2016), and these bubbles could have stripped noble gases from the water in the shallow subsurface. Degassing could also have been caused by pressure reduction during sampling due to the use of a peristaltic pump to retrieve the sample from the spring outlet.

3.3.2 Noble gas recharge temperatures

Modeled estimates of temperature indicate that most samples recharged at 30-33°C, close to the mean annual ground temperature (Table 4). The mean annual air temperature near sample locations is 28.5-30°C (TuTiempo, 2014); ground temperatures are expected to be approximately 3°C higher as that difference is often recorded in arid locations with little vegetative cover (Smith et al., 1964; Beyerle et al., 2003). Wintertime groundwater temperatures at the water table within boreholes have been measured by geophysical well logging at 31.6°C (borehole WDA 16) and 34.8°C (borehole NSHQ 14). These estimates are similar to the previously established 33°C mean annual ground temperature for a more coastal location in Oman (Weyhenmeyer et al., 2000).

Models for most samples with pH > 10 resulted in lower NGTs (Fig. 4). Samples from the two hyperalkaline springs have NGTs between 27°C and 30°C. Samples from the NSHQ 14 borehole have NGTs between 24.6°C and 25.2°C. Unfortunately, it was not possible to model

405 the NGT for borehole NSHQ 04 due to a lack of Kr and Xe data. The NGT for samples from the
406 NSHQ 14 borehole is 6-7 ^{o}C lower than that of our samples from boreholes with modern water.
407 When comparing to modern samples with lower recharge elevations (from SJA 3B and SJA 4B),
408 0.9 ^{o}C of the 7^{o}C NGT difference may be attributed to the 200 m elevation difference, leaving a
409 6.1 ^{o}C difference in recharge temperature unexplained by elevation. Weyhenmeyer et al. (2000)
410 used NGT from groundwater in northern Oman as a paleothermometer and found that during the
411 glacial period of the late Pleistocene (15 ka-25 ka) the mean annual ground temperature was 6.5
412 ^{o}C lower than today. This difference in temperature is similar to the 6-7 ^{o}C difference seen
413 between modern water and that in the NSHQ 14 borehole, so water in NSHQ 14 may have been
414 recharged during a glacial period. The limited rainfall in northern Oman, combined with low
415 permeability within peridotite aquifers may account for the preservation of water recharged
416 during a glacial stage. However, the fact that the Misbit spring has pH > 11 with a modern NGT
417 suggests that waters can develop hyperalkaline compositions without being glacial in age. While
418 it is possible that Misbit spring contains glacial water that has experienced complete
419 reequilibration of noble gases at modern temperature, the high accumulation of helium in this
420 sample implies that it has not recently reequilibrated.

421 *3.4 Non-atmospheric Helium*

422 Figure 5 displays ^{3}He/^{4}He corrected for addition of excess air as a function of the amount of
423 excess helium. All modern samples plot close to the value for water in equilibrium with the
424 atmosphere between lines 1 and 3. These samples have addition of tritiogenic helium but little to
425 no accumulation of crustal or mantle helium.

426 One sample – the Al Hilayw hyperalkaline spring – plots below line 1, which can only be
427 caused by removal of helium through degassing. The removal of helium by degassing in this

428 sample is further supported by the fact that the NGT could only be fit using a model that
429 incorporated fractionation by degassing. As discussed earlier, spring samples may have
430 degassed due to bubbling of hydrogen or methane through the water as it approached the surface.
431 The two samples plotting above line 3 and to the left of solubility equilibrium- borehole
432 NSHQ 04 and the Misbit spring- show significant helium in excess of solubility equilibrium. As
433 both of these samples are pre-bomb, their excess ^{3}He is not from decay of bomb ^{3}H and must
434 therefore be mantle helium. NSHQ 04 has approximately 4% mantle helium, while the Misbit
435 spring has almost 30% mantle helium. The source of mantle helium is likely alteration of the
436 peridotite; some olivine in peridotite samples from the Samail Ophiolite contains 7×10^{-10} to $2 \times$
437 10^{-7} ccSTP/g of He (Mervine, 2012). Mervine (2012) analyzed three olivine samples that had
438 been shielded from cosmogenic radiation and hence production of cosmogenic ^{3}He: all three
439 were enriched in ^{3}He relative to the atmospheric $^{3}He/^{4}He$ ratio and one had a helium ratio similar
440 to mantle helium (1.16×10^{-5}). We do not have a source function for mantle helium in the region,
441 so cannot accurately assess the time it took to accumulate.
442 Samples from borehole NSHQ 14 also have significant helium in excess of solubility
443 equilibrium. The samples plot on line 1, the mixing line between atmospheric helium and *in situ*
444 production or crustal flux of helium. *In situ* production of ^{4}He occurs through the generation of
445 alpha particles during radioactive decay of uranium and thorium in a rock. The average
446 concentration of uranium and thorium in Oman peridotite is 2.3 ppb and 1.2 ppb, respectively
447 (Hanghøj et al., 2010), about one thousand times lower than average crustal concentrations
448 (Taylor, 1964). Given these uranium and thorium concentrations, the *in situ* helium production
449 rate is extremely low. Assuming a porosity of 1% and that all helium produced within the rock
450 is released to aquifer water, accumulation of helium in the peridotite occurs at 1×10^{-13}

ccSTP/yr/g water (e.g., Ballentine et al., 1991). At that rate, it would take 200-220 kyrs to accumulate the levels of excess helium measured in NSHQ 14 samples. If instead the effective porosity is 0.1%, the upper bound measured for upper oceanic crust and a value that implies that flow is isolated within a few channels (Neira et al., 2016), then the amount of He in the water of NSHQ 14 could accumulate in 20-22 kyrs. These age estimates are considered to be upper bounds. Younger water could obtain this level of non-atmospheric He through ^{4}He production and accumulation within peridotite minerals over a long period of time followed by rapid release due to peridotite alteration (cracking of mantle-derived fluid inclusions, dissolution, diffusion). Relatively rapid diffusion of He from aquifer formation rock can occur due to increased surface area (Solomon et al., 1996). In the case of peridotite, surface area may be increased by alteration that produces microfractures at the 10 micron scale (Kelemen et al., 2011). Though $^{3}He/^{4}He$ ratios measured in olivine from the Samail ophiolite were enriched in ^{3}He (Mervine, 2012), local variation did occur and it is possible that in other locations the peridotite contains He enriched in ^{4}He. If peridotite dissolution is primarily responsible for the addition of non-atmospheric He into groundwater, the varying $^{3}He/^{4}He$ ratios in the rock could be responsible for varying $^{3}He/^{4}He$ ratios in the older groundwater samples. Alternatively, crustal fluxes from underlying rock formations with higher uranium and thorium concentrations could also increase ^{4}He in the groundwater more rapidly than *in situ* production. Again, without a source function for local crustal and mantle helium fluxes it is not possible to quantitatively calculate apparent groundwater ages.

However, these helium data are still useful for qualitatively determining relative ages. We can conclude that the five samples with significant helium in excess of solubility equilibrium are older than the samples that have not accumulated non-atmospheric helium. This is particularly

474 useful for water from NSHQ 04, which has no age constraints other than the fact that it is pre-
475 bomb. The water chemistry supports this relative age relationship - the only samples with
476 significant amounts of helium in excess of solubility equilibrium are Type II waters. These
477 waters must be relatively old in order to have attained the level of water-rock interaction
478 necessary to develop this composition. In contrast, all samples with helium concentrations near
479 solubility equilibrium are Type I waters.

480 *3.5 Stable isotopes*

481 $\delta^{18}O$ values in groundwater vary from -2.7 to 1.9‰ VSMOW and $\delta^{2}H$ values vary from -11.2
482 to 6.3‰ VSMOW (Fig. 6). Almost all borehole samples and some hyperalkaline spring samples
483 plot between the Local Meteoric Water Line-North (LMWL-N) and Local Meteoric Water Line-
484 South (LMWL-S) from Weyhenmeyer et al. (2002). Additional hyperalkaline spring samples and
485 borehole samples with pH >11 plot to the right of the LMWL-S, suggesting enrichment in $\delta^{18}O$.
486 It is possible that $\delta^{18}O$ values in groundwater have been altered by peridotite dissolution and CO_2
487 mineralization, and both $\delta^{18}O$ and $\delta^{2}H$ values could have been altered by serpentinization. The
488 effect of low-temperature water-rock interaction on stable isotopes in these fluids remains an
489 open question, and a thorough investigation of this sort is beyond the scope of this paper.
490 Though the following discussion is limited to the effects of water vapor source and evaporation,
491 we do not exclude the possibility of effects from water-rock interaction, particularly in
492 hyperalkaline waters where an extensive amount of water-rock interaction is necessary to
493 generate water of this composition (high Ca^{2+}-OH-, pH > 11).

494 The linear regression line through all samples intersects the LMWL-N at -6.1 ‰ $\delta^{18}O$ and
495 -20.0 ‰ $\delta^{2}H$. This intersection is taken as the starting isotope composition for calculations to
496 estimate the possible effect of evaporation. Rayleigh distillation curves from the starting point

for evaporation at 30°C and humidities of 0% and 50% are shown in Figure 6. While some borehole and spring samples plot along the curve for evaporation at 0% humidity, it is unlikely that the humidity was that low even in an arid environment such as Oman. Weyhenmeyer et al. (2002) estimates the humidity in Northern Oman at 50%. Generating the level of $\delta^{18}O$ enrichment seen in our samples by evaporating at 50% humidity from the starting point along the LMWL-N results in $\delta^{2}H$ enrichment that 5 to 15 ‰ higher than observed. Thus, it is not possible to reach the stable isotope composition of most of our borehole samples through evaporation from a starting point along the LMWL-N. Instead, these waters were likely recharged by a combination of northern and southern vapor sources, as is generally the case for modern Northern Oman groundwater (e.g., Weyhenmeyer et al., 2002; Matter et al., 2005).

Many hyperalkaline spring samples plot around or to the right of the LMWL-S, indicating they have either undergone extensive evaporation from a mixed northern and southern water vapor source, or they have a predominantly southern water vapor source. All samples with NGT < 28°C (hereafter referred to as the low NGTs) plot to the right of the LMWL-S, close to other hyperalkaline waters. This suggests these low NGT samples also may have had a southern water vapor source, and in addition have some enrichment in $\delta^{18}O$ and $\delta^{2}H$ due to evaporation. During the late Pleistocene, the dominant vapor source in northern Oman shifted from the northern, Mediterranean vapor source to the more enriched southerly Indian Ocean vapor source (Weyhenmeyer et al., 2000). This shift may apply to glacial periods in general. If so, groundwater recharged during glacial periods when the southern vapor source prevailed would show a more enriched isotopic signature. A glacial origin is one possible explanation for the $\delta^{18}O$ enrichment of low NGT samples.

4 Conclusions

520 The application of multiple environmental tracers has allowed for some constraints to be
521 placed on the apparent age of groundwater in the Samail Ophiolite. $^{3}H/^{3}He$ dating shows Type I
522 Mg^{2+}-HCO_3^- waters are modern and are inferred to be 0 to 40 years old. Waters with pH > 9.3
523 (generally Type II Ca^{2+}-OH^- water) are pre-bomb with minimal modern mixing. The Type II
524 waters in boreholes and one hyperalkaline spring showed accumulation of helium from both
525 crustal and mantle origins. These apparent ages and water compositions match the expected
526 chemical evolution during serpentinization and CO_2 mineralization predicted by reaction path
527 modeling: samples reflecting greater water-rock interaction have older inferred ages.
528 NGTs for all samples with pH < 10 are between 30°C and 33°C with an average of 32°C,
529 which is consistent with modern recharge. The NGT for the Al Hilayw hyperalkaline spring is
530 5°C lower, or 27°C. NGTs for samples from the only hyperalkaline borehole for which there
531 were noble gas data to fit – NSHQ 14 – modeled without degassing, range from 24.7 to 25.1°C,
532 7°C lower than modern recharge. The NGTs for NSHQ 14 models without degassing correspond
533 to the estimated temperature in Oman during a glacial period in the late Pleistocene
534 (Weyhenmeyer et al., 2000) and suggest these waters are glacial in origin. Stable isotopes for
535 low NGT samples and many hyperalkaline springs are enriched in $\delta^{18}O$, suggesting that they
536 were primarily supplied by the southern vapor source. The southern vapor source was dominant
537 during the last glacial maximum, consistent with the idea of glacial recharge of NSHQ 14
538 samples with low NGTs, and suggesting that water discharged by the hyperalkaline spring at Al
539 Hilayw is also glacial in origin. However, our other hyperalkaline spring sample from Misbit has
540 a modern NGT, indicating that thousands of years are not required to produce Type II waters.
541 Stable isotope data show that most groundwater samples in the ophiolite are comprised of a

mixture between water vapor sources along the LMWL-N and LMWL-S that has lost 0-30% of its water mass due to evaporation.

Unfortunately, it was not possible to assign apparent groundwater ages to any of the samples with pH > 9.3, so the minimum time necessary to generate Type II water by water-rock interaction, and hence the reactive surface area of the peridotite, remains unknown.

5 Future work

Quantitatively determining apparent groundwater age will require more exotic environmental tracers and more sophisticated sampling, e.g., the use of a packer system. Better constraints on apparent groundwater age in the peridotite aquifer may be possible with the collection of a suite of helium data with high spatial and vertical resolution. Establishing a source function for crustal and mantle helium might allow quantitative apparent age determination from helium concentrations in boreholes, rather than just relative age relationships (e.g., Stute et al., 1992). This would be particularly valuable for understanding samples from boreholes NSHQ 14 and NSHQ 04, which have significant excess helium.

The application of ^{39}Ar and ^{81}Kr dating could also help constrain the apparent age of peridotite aquifers in the Samail Ophiolite. ^{39}Ar has a half-life of 269 years, making it ideal for dating waters from a few decades to 1,000 years of age while ^{81}Kr has a half-life of 229,000 years and can be used to date groundwater that is up to 1 Ma (e.g., Loosli et al., 2000, Ritterbusch et al., 2014; Jiang et al., 2017).

Additionally, more noble gas data from borehole and hyperalkaline spring samples could provide greater insight on apparent groundwater age from NGTs. In our dataset, three out of four samples with pH > 10 have low NGTs, but two of these three are from the same borehole.

564 A larger dataset would allow us to determine if this is a coincidence, or if most pH > 10 waters
565 have low NGTs and are glacial in origin.

566 **Acknowledgements**

567 We would like to extend special thanks to the Ministry of Regional Municipalities and Water
568 Resources, Sultanate of Oman, particularly Said Nasser Al Habsi, Dr. Abdulaziz Ali-Al-Mashikhi
569 and Salim Al Khanbashi for providing access to boreholes and physical and chemical data for
570 them. Many thanks to Everett Shock and his students Kirtland Robinson and Peter Marsala at
571 Arizona State University for help in the field, and Dr. Shock's GEOPIG lab for performing trace
572 element analyses. We also thank Peter Schlosser for performing ^{3}H-^{3}He measurements at the
573 Lamont-Doherty Earth Observatory He-Tr Lab.

574 **Funding**

575 This work was supported through the NSF Graduate Research Fellowship Program, Lamont-
576 Doherty Earth Observatory Climate Center, Columbia University Earth Institute Travel Grant
577 Program, Columbia Research Initiative in Science and Engineering, Lamont-Doherty Earth
578 Observatory, Petroleum Development Oman, National Science Foundation Research Grant
579 [MGG-1059175], and Kelemen's Arthur D. Storke Chair at Columbia University. Kelemen's
580 contribution was supported by a National Science Foundation Research Grant [EAR-1049905] and
581 the Storke Chair.

582 **References cited**

583

584 Aeschbach-Hertig, W., Peeters, F., Beyerle, U., & Kipfer, R. (1999). Interpretation of
585 dissolved atmospheric noble gases in natural waters. *Water Resources Research*, *35*(9), 2779-
586 2792.

587

588 Aeschbach-Hertig, W., El-Gamal, H., Wieser, M., & Palcsu, L. (2008). Modeling excess air and
589 degassing in groundwater by equilibrium partitioning with a gas phase. *Water Resources*
590 *Research*, *44*(8).

591

Agrinier, P., Mével, C., & Girardeau, J. (1988). Hydrothermal alteration of the peridotites cored at the ocean/continent boundary of the Iberian margin: petrologic and stable isotope evidence. In *G. Boillot & E.L. Winterer (Eds.), Proceedings of the Ocean Drilling Program Scientific Results, Vol. 103*, (225-234).

Alt, J. C., & Teagle, D. A. (1999). The uptake of carbon during alteration of ocean crust. *Geochimica et Cosmochimica Acta*, 63(10), 1527-1535.

Alt, J. C., Schwarzenbach, E. M., Früh-Green, G. L., Shanks III, W. C., Bernasconi, S. M., Garrido, C. J., ... & Marchesi, C. (2013). The role of serpentinites in cycling of carbon and sulfur: seafloor serpentinization and subduction metamorphism. *Lithos*, 178, 40-54.

Barnes, I., & O'Neil, J. R. (1969). The relationship between fluids in some fresh alpine-type ultramafics and possible modern serpentinization, western United States. *Geological Society of America Bulletin*, *80*(10), 1947-1960.

Ballentine, C. J., O'Nions, R. K., Oxburgh, E. R., Horvath, F., & Deak, J. (1991). Rare gas constraints on hydrocarbon accumulation, crustal degassing and groundwater flow in the Pannonian Basin. *Earth and Planetary Science Letters*, *105*(1), 229-246.

Bruni, J., Canepa, M., Chiodini, G., Cioni, R., Cipolli, F., Longinelli, A., ... & Vetuschi Zuccolini, M. (2002). Irreversible water–rock mass transfer accompanying the generation of the neutral, Mg–HCO_3 and high-pH, Ca–OH spring waters of the Genova province, Italy. *Applied Geochemistry*, *17*(4), 455-474.

Beyerle, U., Rueedi, J., Leuenberger, M., Aeschbach-Hertig, W., Peeters, F., Kipfer, R., & Dodo, A. (2003). Evidence for periods of wetter and cooler climate in the Sahel between 6 and 40 kyr BP derived from groundwater. *Geophysical Research Letters*, 30(4), 22–1-22–4.

Cey, B. D., Hudson, G. B., Moran, J. E., & Scanlon, B. R. (2008). Impact of artificial recharge on dissolved noble gases in groundwater in California. *Environmental science & technology*, *42*(4), 1017-1023.

Chavagnac, V., Monnin, C., Ceuleneer, G., Boulart, C., & Hoareau, G. (2013). Characterization of hyperalkaline fluids produced by low-temperature serpentinization of mantle peridotites in the Oman and Ligurian ophiolites. *Geochemistry, Geophysics, Geosystems*, *14*(7), 2496-2522.

Clark, J. F., Stute, M., Schlosser, P., Drenkard, S., & Bonani, G. (1997). A tracer study of the Floridan aquifer in southeastern Georgia: Implications for groundwater flow and paleoclimate. *Water Resources Research*, *33*(2), 281-289.

Dewandel, B., Lachassagne, P., Boudier, F., Al-Hattali, S., Ladouche, B., Pinault, J. L., & Al-Suleimani, Z. (2005). A conceptual hydrogeological model of ophiolite hard-rock aquifers in Oman based on a multiscale and a multidisciplinary approach. *Hydrogeology Journal*, *13*(5-6), 708-726.

Etiope, G., Tsikouras, B., Kordella, S., Ifandi, E., Christodoulou, D., & Papatheodorou, G. (2013). Methane flux and origin in the Othrys ophiolite hyperalkaline springs, Greece. *Chemical Geology*, *347*, 161-174.

Fisher, A. T., Davis, E. E., Hutnak, M., Spiess, V., Zühlsdorff, L., Cherkaoui, A., Christiansen, L., Edwards, K., Macdonald, R., Villinger, H., Mottl, M.J., Wheat, C.G., & Becker, K. (2003). Hydrothermal recharge and discharge across 50 km guided by seamounts on a young ridge flank. *Nature*, *421*(6923), 618.

Fleitmann, D., & Matter, A. (2009). The speleothem record of climate variability in Southern Arabia. *Comptes Rendus Geoscience*, *341*(8), 633-642.

Hanghøj, K., Kelemen, P. B., Hassler, D., & Godard, M. (2010). Composition and genesis of depleted mantle peridotites from the Wadi Tayin Massif, Oman Ophiolite; major and trace element geochemistry, and Os isotope and PGE systematics. *Journal of Petrology*, *51*(1-2), 201-227.

Heaton, T. H. E., & Vogel, J. C. (1981). "Excess air" in groundwater. *Journal of Hydrology*, *50*, 201-216.

Hutnak, M., Fisher, A. T., Zühlsdorff, L., Spiess, V., Stauffer, P. H., & Gable, C. W. (2006). Hydrothermal recharge and discharge guided by basement outcrops on 0.7–3.6 Ma seafloor east of the Juan de Fuca Ridge: Observations and numerical models. *Geochemistry, Geophysics, Geosystems*, *7*(7).

IAEA (2018). Bahrain Station. Global Network of Isotopes in Precipitation. *International Atomic Energy Agency*, Water Resources Programme. http://www-naweb.iaea.org/napc/ih/IHS_resources_isohis.html Accessed 05/28/2018.

Jiang, W., Yang, G. M., Gu, J. Q., Hu, S. M., & Lu, Z. T. (2017). Radiokrypton dating with Atom Trap Trace Analysis. *Procedia Earth and Planetary Science*, 17, 41-44.

Kelemen, P. B., & Matter, J. (2008). In situ carbonation of peridotite for CO_2 storage. *Proceedings of the National Academy of Sciences*, *105*(45), 17295-17300.

Kelemen, P. B., Matter, J., Streit, E. E., Rudge, J. F., Curry, W. B., & Blusztajn, J. (2011). Rates and mechanisms of mineral carbonation in peridotite: natural processes and recipes for enhanced, *in situ* CO_2 capture and storage. *Annual Review of Earth and Planetary Sciences*, *39*, 545-576.

Le Quéré, C., Andrew, R. M., Canadell, J. G., Sitch, S., Korsbakken, J. I., Peters, G. P., ... & Keeling, R. F. (2016). Global carbon budget 2016. *Earth System Science Data*, *8*(2), 605-649.

Loosli H.H., Lehmann B.E., Smethie W.M. (2000). Noble Gas Radioisotopes: ^{37}Ar, ^{85}Kr, ^{39}Ar, ^{81}Kr. In: Cook P.G., Herczeg A.L. (eds) Environmental Tracers in Subsurface Hydrology. Springer, Boston, MA

Ludin, A., Weppernig,R., Boenisch, G., & Schlosser, P. (1997). Mass spectrometric measurement of helium isotopes and tritium. *Lamont-Doherty Earth Observatory*, Technical Report.

Macumber, P. G. (2003). Lenses, plumes and wedges in the Sultanate of Oman: a challenge for groundwater management. *Developments in Water Science*, *50*, 349-370.

Matter, J. M., Waber, H. N., Loew, S., & Matter, A. (2005). Recharge areas and geochemical evolution of groundwater in an alluvial aquifer system in the Sultanate of Oman. *Hydrogeology Journal*, *14*(1-2), 203-224.

Matter, J. M., Stute, M., Snæbjörnsdottir, S. Ó., Oelkers, E. H., Gislason, S. R., Aradottir, E. S., ... & Axelsson, G. (2016). Rapid carbon mineralization for permanent disposal of anthropogenic carbon dioxide emissions. *Science*, 352(6291), 1312-1314.

Mazor, E. (1972). Paleotemperatures and other hydrological parameters deduced from noble gases dissolved in groundwaters; Jordan Rift Valley, Israel. *Geochimica et Cosmochimica Acta*, *36*(12), 1321-1336.

McGrail, B. P., Schaef, H. T., Spane, F. A., Cliff, J. B., Qafoku, O., Horner, J. A., ... & Sullivan, C. E. (2016). Field validation of supercritical CO2 reactivity with basalts. *Environmental Science & Technology Letters*, 4(1), 6-10.

Mervine, E. M. (2012). Determining timescales of natural carbonation of peridotite in the Samail Ophiolite, Sultanate of Oman. PhD Thesis. Massachusetts Institute of Technology.

Miller, H. M., Matter, J. M., Kelemen, P., Ellison, E. T., Conrad, M. E., Fierer, N., ... & Templeton, A. S. (2016). Modern water/rock reactions in Oman hyperalkaline peridotite aquifers and implications for microbial habitability. *Geochimica et Cosmochimica Acta*, 179, 217-241.

Morrissey, S. K., Clark, J. F., Bennett, M., Richardson, E., & Stute, M. (2010). Groundwater reorganization in the Floridan aquifer following Holocene sea-level rise. *Nature Geoscience*, *3*(10), 683.

Müller, T., Osenbrück, K., Strauch, G., Pavetich, S., Al-Mashaikhi, K. S., Herb, C., ... & Sanford, W. (2016). Use of multiple age tracers to estimate groundwater residence times and long-term recharge rates in arid southern Oman. *Applied Geochemistry*, 74, 67-83.

Neal, C., & Stanger, G. (1983). Hydrogen generation from mantle source rocks in Oman. *Earth and Planetary Science Letters*, *66*, 315-320.

Neal, C., & Stanger, G. (1985). Past and present serpentinisation of ultramafic rocks; an example from the Semail Ophiolite Nappe of Northern Oman. In: Drever, J. I. (Ed.), *The Chemistry of Weathering*, D. Reidel Publishing, 249-275.

Neira, N. M., Clark, J. F., Fisher, A. T., Wheat, C. G., Haymon, R. M., & Becker, K. (2016). Cross-hole tracer experiment reveals rapid fluid flow and low effective porosity in the upper oceanic crust. *Earth and Planetary Science Letters*, *450*, 355-365.

Nicolas, A., Boudier, E., Ildefonse, B., & Ball, E., (2000). Accretion of Oman and United Arab Emirates ophiolite: discussion of a new structural map. *Marine Geophysical Researches* 21 (3–4), 147–179.

Paukert, A. N., Matter, J. M., Kelemen, P. B., Shock, E. L., & Havig, J. R. (2012). Reaction path modeling of enhanced *in situ* CO_2 mineralization for carbon sequestration in the peridotite of the Samail Ophiolite, Sultanate of Oman. *Chemical Geology*, *330*, 86-100.

Paukert, A. N. (2014). *Mineral Carbonation in Mantle Peridotite of the Samail Ophiolite, Oman: Implications for permanent geological carbon dioxide capture and storage*. Ph.D. Thesis. Columbia University, New York, NY. https://doi.org/10.7916/D85M63WZ.

Ritterbusch, F., Ebser, S., Welte, J., Reichel, T., Kersting, A., Purtschert, R., Aeschbach-Hertig, W., & Oberthaler, M.K. (2014). Groundwater dating with Atom Trap Trace Analysis of ^{39}Ar. *Geophysical Research Letters*, 41(19), 6758-6764.

Rozanski, K., Gonfiantini, R., & Araguas-Araguas, L. (1991). Tritium in the global atmosphere: Distribution patterns and recent trends. *Journal of Physics G: Nuclear and Particle Physics*, *17*(S), S523.

Rozanski, K., Araguas-Araguas, L., & Gonfiantini, R. (1993). Isotopic Patterns in Modern Global Precipitation. In P. K. Swart, K. C. Lohmann, J. McKenzie, & S. Savin (Eds.), *Climate Change in Continental Isotopic Records.* Washington DC American Geophysical Union Geophysical Monograph Series, *78*.

Schwarzenbach, E. M., Früh-Green, G. L., Bernasconi, S. M., Alt, J. C., & Plas, A. (2013). Serpentinization and carbon sequestration: A study of two ancient peridotite-hosted hydrothermal systems. *Chemical Geology*, 351, 115-133.

Smith, G. D., Newhall, F., Robinson, L. H., & Swanson, D. (1964). Soil-temperature regimes their characteristics and predictability. *U.S. Department of Agriculture.* SCS-TP-144.

Snæbjörnsdóttir, S. Ó., Oelkers, E. H., Mesfin, K., Aradóttir, E. S., Dideriksen, K., Gunnarsson, I., ... & Gislason, S. R. (2017). The chemistry and saturation states of subsurface fluids during the in situ mineralisation of CO 2 and H 2 S at the CarbFix site in SW-Iceland. *International Journal of Greenhouse Gas Control*, 58, 87-102.

776 Solomon, D. K. (1992). The use of tritium and helium isotopes to determine groundwater
777 recharge to unconfined aquifers. PhD thesis. University of Waterloo, Waterloo, Ontario,
778 Canada
779
780 Solomon, D. K., Hunt, A., & Poreda, R. J. (1996). Source of radiogenic helium 4 in shallow
781 aquifers: Implications for dating young groundwater. *Water Resources Research*, 32(6),
782 1805-1813.
783
784 Stute, M., Sonntag, C., Déak, J., & Schlosser, P. (1992). Helium in deep circulating
785 groundwater in the Great Hungarian Plain: Flow dynamics and crustal and mantle helium
786 fluxes. *Geochimica et Cosmochimica Acta*, *56*(5), 2051-2067.
787
788 Stute, M., & Schlosser, P. (1993). Principles and applications of the noble gas paleothermometer.
789 *Climate Change in Continental Isotopic Records*, 89-100.
790
791 Stute, M., Forster, M., Frischkorn, H., Serejo, A., Clark, J. F., Schlosser, P., ... & Bonani, G.
792 (1995). Cooling of Tropical Brazil (5 C) During the Last Glacial Maximum. *Science*
793 269(5222). 379-379.
794
795 Taylor, S. R. (1964). Abundance of chemical elements in the continental crust: a new table.
796 *Geochimica et Cosmochimica Acta*, *28*(8), 1273-1285.
797
798 Tolstikhin, I.N., & Kamensky, I.L. (1969). Determination of groundwater ages by the T-^{3}He
799 method. *Geochemistry International 6,* 810-811.
800
801 Torgersen, T., & Ivey, G. N. (1985). Helium accumulation in groundwater. II: A model for the
802 accumulation of the crustal ^{4}He degassing flux. *Geochimica et Cosmochimica Acta*, *49*(11),
803 2445-2452.
804
805 Torgersen, T., & Stute, M. (2013). Helium (and other Noble Gases) as a Tool for Understanding
806 Long Timescale Groundwater Transport. In *Isotope Methods for Dating Old Groundwater*
807 (179-216). Vienna, Austria: International Atomic Energy Agency.
808
809 TuTiempo.net. Climate Oman. http://www.tutiempo.net/en/Climate/Oman/OM.html. 02/19/14.
810
811 Weiss, R. F. (1968, December). Piggyback sampler for dissolved gas studies on sealed water
812 samples. *Deep Sea Research and Oceanographic Abstracts*, *15*(6), 695-699.
813
814 Weyhenmeyer, C. E., Burns, S. J., Waber, H. N., Aeschbach-Hertig, W., Kipfer, R., Loosli, H.
815 H., & Matter, A. (2000). Cool glacial temperatures and changes in moisture source recorded
816 in Oman groundwaters. *Science*, *287*(5454), 842-845.
817
818 Weyhenmeyer, C. E., Burns, S. J., Waber, H. N., Macumber, P. G., & Matter, A. (2002). Isotope
819 study of moisture sources, recharge areas, and groundwater flow paths within the eastern
820 Batinah coastal plain, Sultanate of Oman. *Water Resources Research*, *38*(10), 2-1.
821

Wheat, C. G., Elderfield, H., Mottl, M. J., & Monnin, C. (2000). Chemical composition of basement fluids within an oceanic ridge flank: Implications for along-strike and across-strike hydrothermal circulation. *Journal of Geophysical Research: Solid Earth*, 105(B6), 13437-13447.

Winslow, D. M., Fisher, A. T., Stauffer, P. H., Gable, C. W., & Zyvoloski, G. A. (2016). Three-dimensional modeling of outcrop-to-outcrop hydrothermal circulation on the eastern flank of the Juan de Fuca Ridge. *Journal of Geophysical Research: Solid Earth*, 121(3), 1365-1382.

Table 1: Field data for borehole samples

Borehole	UTM Coordinates WGS 84 datum		Well depth	Screened interval depth	Sample ID	Sampling depth	pH	Temp.	EC	ORP
	Easting	Northing	mbtoc[a]	mbtoc		mbtoc		°C	µS/cm	mV
Deep boreholes[b]										
NSHQ 14	0675491	2529716	304	open > 6	12_03M	15	10.01	28.7	1491	-31.6
					12_03N	70	11.03	31.6	2710	-103.4
					12_03O	260	11.05	28.1	2770	-597.3
NSHQ 04	0670975	2531692	304	open > 6	12_04P	70	10.62	27.0	3330	-261.7
WDA 16	0528580	2539767	350	23-139, open > 145	12_05Q	50	7.93	33.6	461	N/A
					12_05R	243	7.81	32.2	470	N/A
					12_05S	298	7.92	34.5	472	N/A
WDA 17	0522099	2550048	350	25-31, 37-63, open > 69	12_06T	160	9.10	30.7	508	93.3
WDA 05	0526133	2539283	203	23-27, 39-47, 101-148, open > 156	12_08Y	65	9.05	33.1	568	97.7
					12_08Z	140	9.11	31.1	585	77.7
Shallow boreholes[c]										
SJA 4B	0601942	2582989	53	17-49	10_11AX	18	7.23	33.8	598	201
SJA 4A	0601962	2582964	20	4-16	10_11AY	14	7.57	34.0	491	164
SJA 3B	0602847	2582068	38	20-36	10_11AZ[d]	18	9.36	34.1	586	94

[a] All depth measurements given in meters below top of casing

[b] Samples collected with point-source bailer

[c] Samples collected with typhoon pump

[d] Previously reported in Paukert et al. (2012)

Table 2: Major ion chemistry and trace element concentrations for boreholes and hyperalkaline springs sampled for noble gases[a]

Sample ID	Location	Cl^-	NO_3^-	SO_4^{2-}	DIC	OH^{-b}	Ca^{2+}	Na^+	K^+	$Mg^{2+\,c}$	Si^{4+}	$Al^{3+\,d,e}$	$Fe^{2+\,d,e}$	U^d	Th^d
Deep boreholes															
12_03M	NSHQ 14	4.68	0.02	0.12	0.08	0.28	1.23	2.54	0.10	3.87E-02	<0.02	5.19E-04	1.54E-05	<4E-08	<2E-08
12_03N	NSHQ 14	15.81	<0.01	0.01	0.09	3.98	4.11	11.65	0.28	1.48E-02	<0.02	4.56E-04	4.66E-06	<4E-08	<2E-08
12_03O	NSHQ 14	14.34	<0.01	0.03	0.08	4.10	3.81	10.32	0.26	1.56E-02	<0.02	3.71E-04	8.99E-06	<4E-08	<2E-08
12_04P	NSHQ 04	38.73	<0.01	0.12	0.39	1.05	13.71	14.00	0.42	2.80E-02	<0.02	7.45E-04	3.40E-05	<4E-08	<2E-08
12_05Q	WDA 16	0.77	0.20	0.31	2.94	0	0.43	1.19	0.06	1.47	0.44	N/A	N/A	N/A	
12_05R	WDA 16	0.77	0.19	0.31	2.93	0	0.44	1.21	0.06	1.45	0.46	N/A	N/A	N/A	
12_05S	WDA 16	0.79	0.20	0.31	2.98	0	0.44	1.22	0.06	1.47	0.45	3.41E-04	1.97E-04	5.9E-08	<2E-08
12_06T	WDA 17	1.13	0.09	0.73	2.48	0	0.05	0.87	0.04	2.35	<0.02	2.93E-04	6.41E-06	<4E-08	<2E-08
12_08Y	WDA 05	2.06	0.13	0.73	1.82	0	0.05	1.37	0.07	2.32	<0.02	9.64E-05	1.67E-05	<4E-08	<2E-08
12_08Z	WDA 05	2.02	0.13	0.72	1.75	0	0.05	1.37	0.07	2.33	<0.02	1.19E-04	9.13E-06	<4E-08	<2E-08
Hyperalkaline springs[f]															
09_W02A	Falaij													1.2E-07	<2E-08
09_W04F	Al Hilayw													<4E-08	<2E-08
09_W06O	Dima													<4E-08	<2E-08
09_W10U	Misbit													5.9E-08	<2E-08
09_W13D	Shumayt													<4E-08	<2E-08
Shallow boreholes															
10_11AX	SJA 4B	1.12	0.19	0.37	3.98	0.28	1.23	1.12	0.05	1.23	0.39	<5 E-04	<2 E-05	8.2E-06	<2E-08
10_11AY	SJA 4A	0.72	0.18	0.26	3.50	3.98	1.07	0.71	0.05	1.22	0.43	<5 E-04	2.58E-05	1.8E-06	<2E-08
10_11AZ	SJA 3B	2.05	0.09	0.89	1.42	4.10	0.05	1.43	0.07	2.23	<0.02	<5 E-04	<2 E-05	<4E-08	<2E-08

[a] All concentrations given in mmol/l

[b] OH^- from field alkalinity titrations

[c] Mg values below 1 mmol/l are from ICP-MS, others are ICP-AAS

[d] All values from ICP-MS

[e] Detection limits were higher for 2010 samples (10_11AX-AZ)

[f] Solute concentrations other than U for these springs all previously reported in Paukert et al. (2012)

Table 3: Dissolved noble gas concentrations[a]

Sample	Location	pH	He	Ne	Ar	Kr	Xe	^{3}He	R_{Ne}[c]
Deep Boreholes									
12_03N1	NSHQ 14	11.03	1.05E-07	3.14E-07	3.45E-04	6.75E-08	8.19E-09	1.25E-13	1.93
12_03N2[d]	NSHQ 14	11.03	9.60E-08	2.88E-07	3.20E-04	6.60E-08	8.07E-09	9.80E-14	1.74
12_03O2	NSHQ 14	11.05	9.15E-08	2.65E-07	3.10E-04	6.50E-08	8.07E-09	9.48E-14	1.60
12_04P1	NSHQ 04	10.60	1.46E-07	2.93E-07	2.83E-04	N/A	N/A	1.67E-13	1.95
12_05Q	WDA 16	7.93	5.37E-08	2.05E-07	2.52E-04	5.24E-08	6.39E-09	7.16E-14	1.32
12_05R1	WDA 16	7.81	5.07E-08	1.92E-07	2.47E-04	5.12E-08	6.30E-09	8.12E-14	1.24
12_05S1	WDA 16	7.92	4.39E-08	1.89E-07	2.42E-04	4.96E-08	6.38E-09	6.57E-14	1.21
12-05S3[d]	WDA 16	7.92	4.76E-08	1.95E-07	2.38E-04	5.05E-08	6.14E-09	6.94E-14	1.25
12-06T1	WDA 17	9.10	5.16E-08	2.13E-07	2.54E-04	5.40E-08	6.56E-09	8.39E-14	1.36
12_08Y1	WDA 05	9.05	6.12E-08	2.41E-07	2.74E-04	5.45E-08	6.95E-09	1.12E-13	1.52
12_08Z1	WDA 05	9.11	5.01E-08	1.92E-07	2.48E-04	5.18E-08	6.39E-09	7.65E-14	1.23
09_W02A	Falaij	11.52	1.90E-08	6.65E-08	1.57E-04	3.91E-08	5.43E-09	2.37E-14	0.44
09_W04F	Al Hilayw	11.59	3.86E-08	1.44E-07	2.32E-04	5.14E-08	6.84E-09	4.65E-14	1.02
09_W06O	Dima	11.45	3.58E-08	1.39E-07	2.33E-04	5.07E-08	6.62E-09	4.54E-14	0.87
09_W10U	Misbit	11.20	7.88E-08	1.95E-07	2.62E-04	5.45E-08	6.99E-09	1.72E-13	1.20
09_W13D	Shumayt	11.46	2.59E-08	4.16E-08	1.41E-04	3.43E-08	4.85E-09	3.44E-14	0.27
Shallow boreholes									
10-11AX1	SJA 4B	7.23	5.27E-08	2.11E-07	2.61E-04	5.24E-08	6.62E-09	6.52E-14	1.32
10-11AX2[d]	SJA 4B	7.23	5.44E-08	2.13E-07	2.66E-04	5.33E-08	6.64E-09	7.62E-14	1.33
10-12AZ1	SJA 3B	9.36	5.48E-08	2.21E-07	2.71E-04	5.35E-08	6.67E-09	8.84E-14	1.38
10-12AZ2[d]	SJA 3B	9.36	5.56E-08	2.17E-07	2.72E-04	5.38E-08	6.69E-09	8.61E-14	1.36

[a] All noble gas concentrations given in ccSTP/g water

[b] For borehole samples depth is given in meters below top of casing

[c] R_{Ne} is given by $Ne_{sample}/Ne_{solubility\ equilibrium}$

[d] Field replicate

Table 4: Noble gas thermometry modeling parameters and results

Sample ID	Location	Recharge elevation	NOBLE90 model[a]	Probability of fit[b]	Excess air	Recharge temp.	Recharge temp. uncertainty[c]
		m		%	ccSTP/g	°C	°C
Deep Boreholes							
12_03N1	NSHQ 14	620	TA-1	2.5	8.34E-03	24.95	0.62
12_03N2[d]	NSHQ 14	620	TA-1	1.9	6.74E-03	25.14	0.63
12_03O2	NSHQ 14	620	TA-1	3.2	5.46E-03	24.67	0.57
12_04P1	NSHQ 04	600	N/A	N/A	7.84E-03	N/A	N/A
12_05Q	WDA 16	680	TA-1	7.0	2.70E-03	32.11	0.53
12_05R1	WDA 16	680	TA-1	18.4	2.05E-03	32.32	0.41
12_05S1	WDA 16	680	TA-1	12.0	1.83E-03	32.59	0.46
12_08Y1	WDA 05	660	TA-1	8.5	4.52E-03	30.72	0.52
12_08Z1	WDA 05	660	TA-1	15	1.97E-03	31.84	0.43
Hyperalkaline Springs							
09_W04F	Al Hilayw	560	TAF-3	85.5	1.62E-04	27.14	0.16
09_W10U	Misbit	440	TA-1	91.1	1.76E-03	29.70	0.09
Shallow boreholes							
10-11AX1	SJA 4B	420	TA-1	78.3	2.79E-03	32.61	0.16
10-11AX2[d]	SJA 4B	420	TA-1	70.1	2.87E-03	32.14	0.19
10-12AZ1	SJA 3B	420	TA-1	40.6	3.35E-03	32.21	0.31
10-12AZ2[d]	SJA 3B	420	TA-1	19.0	3.16E-03	31.85	0.42

[a] NOBLE90 models are described in detail in the NOBLE90 manual. TA-1 is a closed system equilibration model with temperature and excess air as free parameters, TAF-3 is a partial degassing model with temperature, excess air, and fractionation as free parameters.

[b] Samples with less than 1% probability of fit are excluded

[c] Determined by NOBLE90, scaled to account for model goodness of fit

[d] Field replicate

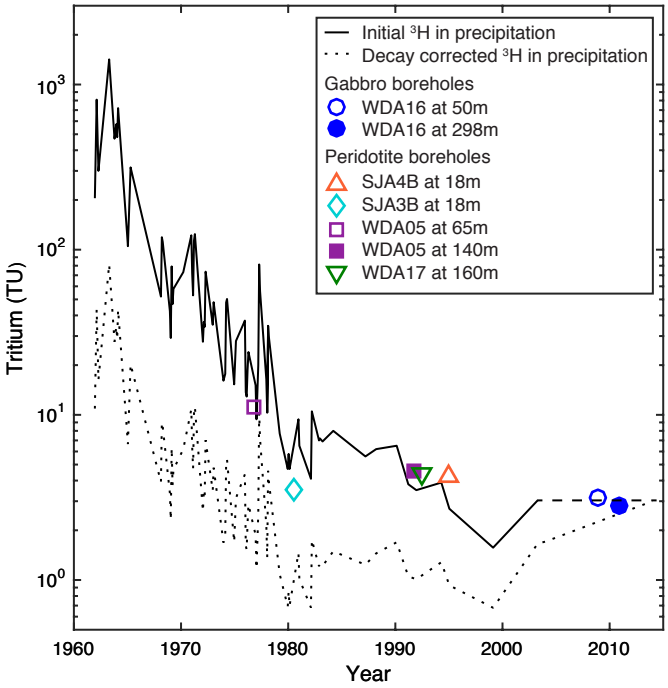

Figure 1: ^3H in local precipitation and borehole water samples. Solid black line is initial ^3H concentration in precipitation measured at Bahrain IAEA/WMO GNIP station 4115001, with inferred concentration of 3 TU in recent precipitation. Dashed line is ^3H in precipitation decay corrected for January 1, 2014. Note that decay corrected ^3H concentrations would be similar for precipitation that fell between 1980 and 2000. Symbols show calculated $^3H_{initial}$ vs recharge year determined by $^3H/^3He$ dating of modern groundwater samples.

Figure 2: Locations of hyperalkaline springs and boreholes sampled for noble gases in the Samail ophiolite.

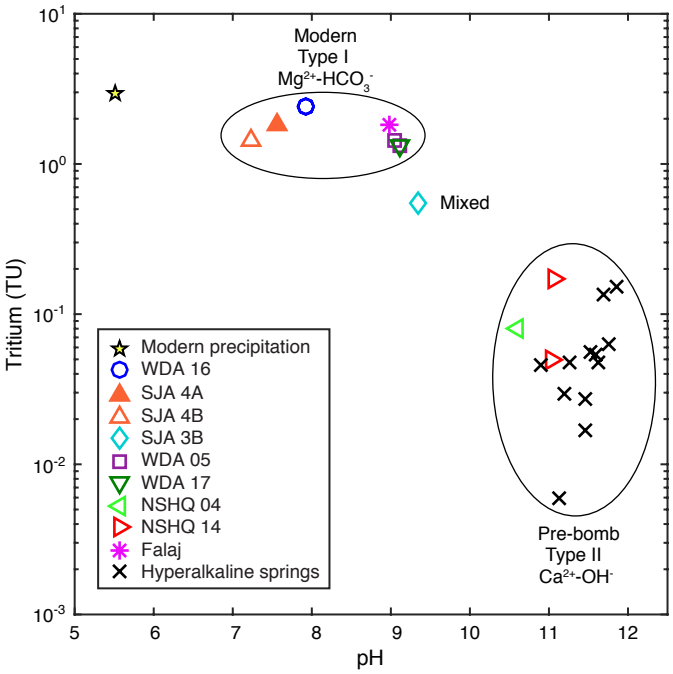

Figure 3: Measured ^3H in samples. Samples with Type I Mg^{2+}-HCO_3^- water have > 0.6 TU and are considered modern (recharged after 1952). Samples with Type II Ca^{2+}-OH^- water have < 0.6 TU and are considered pre-bomb (recharged prior to 1952) with less than 10% modern water mixed in. One sample appears to contain a mixture of modern and pre-bomb water. Detection limit is 5×10^{-3} TU.

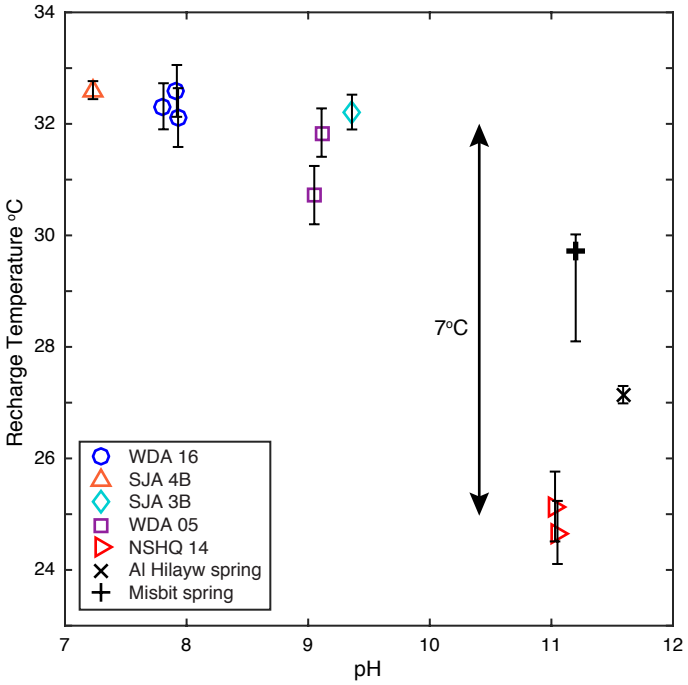

Figure 4: Recharge temperatures modeled from noble gases. The larger and asymmetric error associated with the Misbit spring value is due to a larger uncertainty in recharge elevation. Mean annual ground temperature is estimated at 33°C.

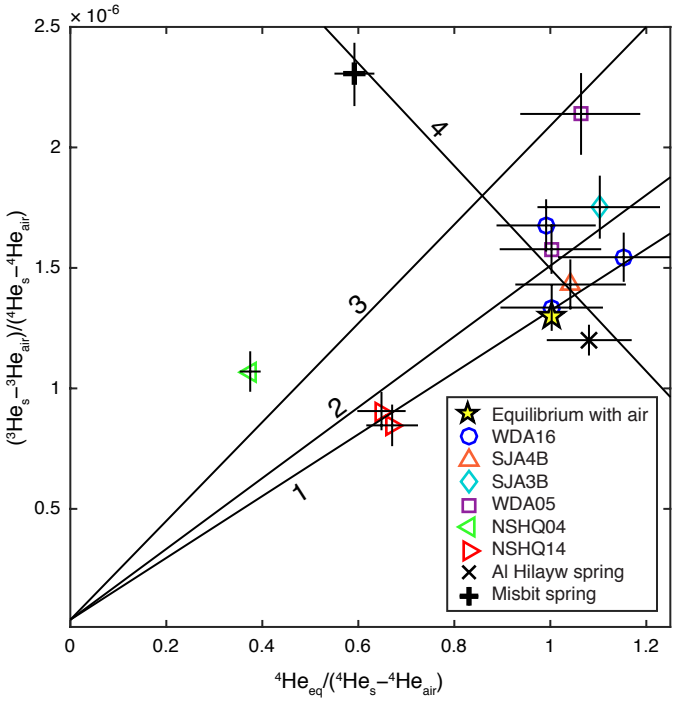

Figure 5: $^3He/^4He$ ratio in samples corrected for excess air as a function of the amount of excess helium, where ^3He_s and ^4He_s are the concentrations measured in the sample, $^3He_{air}$ and $^4He_{air}$ are the concentrations due to excess air, and $^4He_{eq}$ is the concentration at solubility equilibrium with air (after Stute et al., 1992). Line 1 is a mixing line between water saturated with atmospheric helium and crustal helium or helium produced *in situ*. Addition of tritiogenic ^3He from decay of 3 TU (as in pre-bomb recharge) shifts line 1 to line 2. Addition of ^3He from decay of 12 TU (as in 1977 recharge, the age of our oldest sample datable by ^3H-^3He) shifts line 1 to line 3. Addition of 30% mantle helium shifts line 2 to line 4.

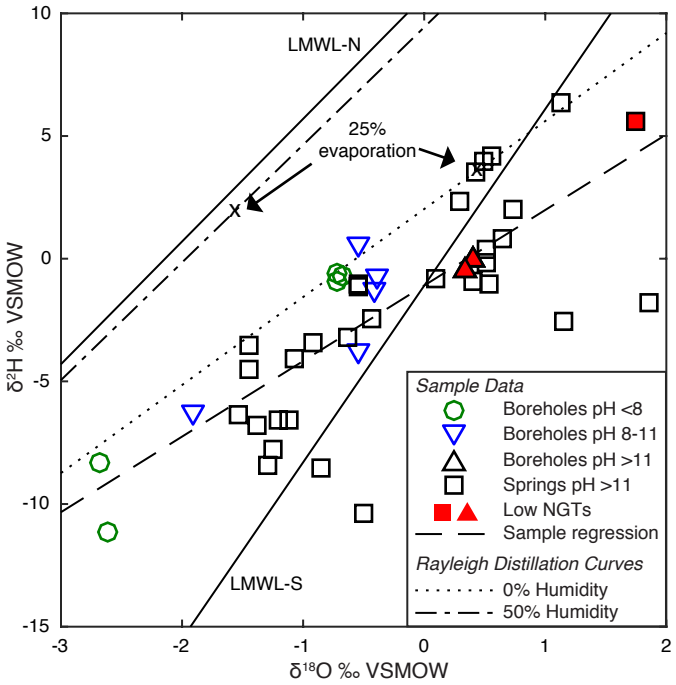

Figure 6: Stable isotopes in all samples. Samples with noble gas temperatures less than 28°C (low NGT) are filled with red. Local Meteoric Water Line - North and -South are taken from Weyhenmeyer et al. (2002). Dashed black line represents a linear regression for all samples. Dotted lines represent Rayleigh distillation at 30°C for 0% or 50% humidity from the point at which the sample regression line intersects the LMWL-N. Xs indicate 25% evaporation from the starting point.

Supporting Information

Multitracer determination of apparent groundwater ages in peridotite aquifers within the Samail ophiolite, Sultanate of Oman

Amelia N. Paukert Vankeuren[a,b], Jürg M. Matter[a,c], Martin Stute[a,d], Peter B. Kelemen[a,e]

[a]Lamont-Doherty Earth Observatory, Columbia University, 61 Route 9W, Palisades, NY 10964
[b]Geology Department, California State University, Sacramento, 6000 J Street, M/S 6043, Sacramento CA 95819
[c]Ocean and Earth Science, National Oceanography Centre Southampton, University of Southampton, UK
[d]Department of Environmental Science, Barnard College, 3009 Broadway, 404 Altschul Hall, New York, NY 10027
[e]Department of Earth and Environmental Sciences, Columbia University, New York, NY 10027

Noble gases

Noble gas concentrations were modeled using the Matlab routine NOBLE90 utilizing temperature, excess air, and fractionation due to partial dissolution, re-equilibration and degassing as free parameters (Aeschbach-Hertig et al., 1999). For our models, fixed input parameters were salinity, pressure, and measured concentrations plus error estimates for neon, argon, krypton, and xenon. Salinity was set to 0.42‰, the expected composition at the time of recharge, representing a mixture between precipitation and local surface water with a typical salinity of 0.84‰ (Paukert et al., 2012). The pressure at the recharge point was determined from the median elevation for its catchment as estimated from topographic maps. The Weiss solubility dataset was employed (Weiss 1970; Weiss, 1971; Smith and Kennedy, 1983). The model selected for each sample was the simplest model that provided acceptable probability (>1%) as recommended by Aeschbach-Hertig et al. (1999). For all samples but one, this was the model that used temperature and excess air as free parameters. The probability of this model fitting the borehole water dataset as a whole was two orders of magnitude higher than that of any other model, which further supports the choice of this model for calculating recharge

temperatures. The hyperalkaline spring sample 09_W04F required a model incorporating fractionation due to partial degassing to obtain an acceptable probability.

Sensitivity analysis was conducted for elevation, salinity, and model free parameters. For elevation, NOBLE90 was run for each sample using three different elevations: the elevation of the sample site itself, which can be taken as the minimum possible recharge elevation, the median elevation in the catchment, and the maximum elevation in the catchment. The range of possible recharge elevations generally differed by less than 300m, though the Misbit spring has a recharge elevation range of over 600m. Within these elevation ranges, the difference in modeled excess air components and NGTs for each sample differed by less than 14% and 1.5°C, respectively, with lower elevations resulting in higher temperatures. One exception was the Misbit spring, where the excess air and NGT varied by 30% and 3.3°C, respectively, due to differences in recharge elevation. The uncertainty in recharge temperatures due to salinity variation within the range from pure precipitation (0‰) to local surface water (0.84‰) is $\pm$0.2 °C, with higher temperatures resulting from lower salinity. Each sample was run for models incorporating the various free parameters. Recharge temperatures varied by at most 2°C depending on the model, with the degassing model producing the lowest temperatures and the partial reequilibration model producing the highest. It should be noted that all of these parameters - elevation, salinity, and model choice - introduce uncertainty into the NGT dataset, but each factor acts in the same direction for all of the samples so the relative differences between samples remain. Thus, conclusions regarding modern vs. glacial NGTs are unaffected by the final selection of input parameters and modeled free parameters.

Radiocarbon dating

Radiocarbon samples were collected using a point-source stainless steel bailer (Model 429, Solinst, Georgetown, ON, Canada) with ball valves at the top and bottom to seal the bailer and prevent mixing with shallower water as it returned to the surface. At the surface, samples were poured into 500 ml or 1 liter amber glass bottles containing a small amount of mercuric chloride. Radiocarbon was measured by the National Ocean Sciences Accelerator Mass Spectrometry Facility at the Woods Hole Oceanographic Institution with an error of less than 1 % modern carbon.

Radiocarbon values in boreholes range from 20% to 98% modern carbon, while springs range from 82% to 101% modern carbon (Table S1). Hyperalkaline springs and hyperalkaline boreholes are probably artificially enriched in modern radiocarbon due to absorption of modern CO_2 in the shallow subsurface or from the atmosphere during the sampling process. Due to the very low dissolved carbon content and hyperalkaline pH, samples may have rapidly absorbed atmospheric CO_2 causing the carbon signal to be dominated by the modern component.

These radiocarbon values should not be taken as accurate assessments of groundwater age. They have not been corrected for changes that may have occurred along the flow path due to chemical reactions such as dissolution of carbonate minerals. A model for radiocarbon alteration along the groundwater flow path will need to be developed in order to estimate ages of these waters.

Table S1: Tritium and stable isotope data for all water samples

Sample ID	Location	UTM Coord. (WGS 84) Easting	Northing	Depth[a] mbtoc	pH	$\delta^{18}O$ ‰	$\delta^{2}H$ ‰	^{3}H[b] TU	Age yrs	^{3}H % modern	^{14}C % modern
Deep boreholes											
12_03N	NSHQ 14	0675491	2529716	70	11.03	0.41	-0.08	*0.050*	> 60	1.7	
12_03O	NSHQ 14	0675491	2529716	260	11.05	0.34	-0.49	*0.170*	> 60	5.7	94.2
12_04P	NSHQ 04	0670975	2531692	70	10.60	-1.92	-6.27	*0.080*	> 60	2.7	24.6
12_05Q	WDA 16	0528569	2539772	50	7.93	-0.68	-0.76	2.390	4.1[c]		
12_05R	WDA 16	0528569	2539772	243	7.81	-0.72	-0.88	2.360	4.3[c]		
12_05S	WDA 16	0528569	2539772	298	7.92	-0.71	-0.55	2.380	4.2[c]		98.2
12_06T	WDA 17	0522099	2550048	160	9.10	-0.54	0.56	1.330	21.5		20.5
12_08Y	WDA 05	0526133	2539283	65	9.05	-0.38	-0.71	1.410	37.3		
12_08Z	WDA 05	0526133	2539283	140	9.11	-0.41	-1.26	1.320	22.2		
Shallow boreholes											
10_11AX	SJA 4B	0601942	2582989	18	7.23	-2.62	-11.17	1.438	13.2[c]		
10_11AY	SJA 4A	0601962	2582964	14	7.57	-2.68	-8.33	1.817	9.0[c]		
10_12AZ	SJA 3B	0602847	2582068	18	9.36	-0.55	-3.71	0.546	> 60	18.2	
Hyperalkaline springs											
09_W02A	Falaij	0608436	2525957	0							
09_W04F	Al Hilayw	0585875	2523231	0	11.59	1.74	5.64	*0.053*	> 60	1.8	
09_W04G	Al Hilayw	0585877	2523246	0	11.27	2.02	6.02	*0.048*	> 60	1.6	
09_W04H	Al Hilayw	0585582	2523248	0	11.51	2.50	9.75				
09_W05L	Qafifah	0646070	2533683	0	11.89	0.39	-0.92				
09_W06O	Dima	0663442	2542614	0	11.45	0.52	-0.14	*0.017*	> 60	0.6	
09_W10U	Misbit	0625997	2576261	0	11.20	-1.11	-6.63	*0.029*	> 60	1.0	81.9
09_W12Z	Sudari	0442831	2649842	0	11.64	-1.29	-8.41				

[a] For borehole samples depth is given in meters below top of casing

[b] Italics used to show samples with greater than 5% error

[c] Ages calculated using Eq. 3. All other ages calculated using Eq. 4.

Table S1 continued: Tritium and stable isotope data for all water samples

		UTM Coord. (WGS 84)		Depth[a]	pH	$\delta^{18}O$	$\delta^{2}H$	^{3}H[b]	Age	^{3}H	^{14}C
Sample ID	Location	Easting	Northing	mbtoc		‰	‰	TU	yrs	% modern	% modern
Hyperalkaline springs											
09_W13D	Shumayt	0486044	2588467	0	11.46	-1.46	-4.51	*0.027*	> 60	0.9	93.3
09_W14H	Al Bana	0487587	2575971	0	12.08	0.54	-1.04				
09_W14I	Al Bana	0487342	2576124	0	11.84	1.86	-1.79	0.154	> 60	5.1	
09_W15J	Uqayba	0427059	2634133	0	11.25	-1.20	-6.60				
09_W15K	Uqayba	0426221	2633900	0	11.68	-0.86	-8.49				
09_W16M	Sudari	0443118	2650291	0	11.90	-0.49	-10.36				
10_01A	Misbit	0625997	2576261	0	11.20	-1.39	-6.75				
10_02L	Falaij	0608436	2525957	0	11.52	0.65	0.85				
10_03R	Falaij 2	0608561	2526486	0	11.63	1.12	6.33				
10_04S	Qafifah	0646115	2533648	0	11.76	0.56	4.14	*0.064*	> 60	2.1	
10_04U	Qafifah	0646071	2533679	0	11.76	0.28	2.38				
10_05AA	Al Bana	0487584	2575976	0	11.71	0.09	-0.85				
10_05AD	Al Bana	0487338	2576123	0	11.68	1.15	-2.59	*0.137*	> 60	4.6	
10_05AF	Al Bana	0487951	2575513	0	11.90	0.51	0.38				100.6
10_06AG	Al Bana	0489557	2575443	0	11.14	-0.42	-2.40	*0.006*	> 60	0.2	95.5
10_06AH	Al Bana	0489564	2575430	0	11.16	-1.08	-4.08				96.8
10_07AJ	Shumayt	0486044	2588467	0	11.46	-1.44	-3.49				
10_09AT	Sudari	0443118	2650087	0	11.61	-1.54	-6.36				
10_10AV	Uqayba	0426225	2633900	0	11.61	-1.24	-7.81	*0.048*	> 60	1.6	
12_01G	Falaij	0608436	2525957	0	11.25	-0.53	-1.16				
12_02L	Falaij	0608561	2526486	0	11.21	-0.54	-1.08				
12_07X	Al Bana	0487951	2575513	0	11.60	-0.62	-3.23				

[a] For borehole samples depth is given in meters below top of casing

[b] Italics used to show samples with greater than 5% error

References cited:

Aeschbach-Hertig, W., Peeters, F., Beyerle, U., & Kipfer, R. (1999). Interpretation of dissolved atmospheric noble gases in natural waters. *Water Resources Research*, *35*(9), 2779-2792.

Paukert, A. N., Matter, J. M., Kelemen, P. B., Shock, E. L., & Havig, J. R. (2012). Reaction path modeling of enhanced *in situ* CO_2 mineralization for carbon sequestration in the peridotite of the Samail Ophiolite, Sultanate of Oman. *Chemical Geology*, *330*, 86-100.

Smith, S. P., & Kennedy, B. M. (1983). The solubility of noble gases in water and in NaCl brine. *Geochimica et Cosmochimica Acta*, *47*(3), 503-515.

Weiss, R. F. (1970, August). The solubility of nitrogen, oxygen and argon in water and seawater. *Deep Sea Research and Oceanographic Abstracts*, *17*(4), 721-735.

Weiss, R. F. (1971). Solubility of helium and neon in water and seawater. *Journal of Chemical & Engineering Data*, *16*(2), 235-241.